Photon-by-Photon Determination of Emission Bursts from Diffusing Single Chromophores

Kai Zhang and Haw Yang*

Department of Chemistry, University of California at Berkeley, and Physical Biosciences Division, Lawrence Berkeley National Laboratory, Berkeley, California 94720

Received: August 16, 2005; In Final Form: September 22, 2005

One of the difficulties in diffusion-type single-molecule experiments is the determination of signal amid photon-counting noise. A commonly used approach is to further average the noisy time trace by binning, followed by placing a threshold to discriminate signal from background. The choice of smoothing parameters and the placement of the threshold may impact on the efficiency with which the information-rich region can be harvested, among other potential complications. Here we introduce a procedure that operates on the data sequence photon by photon, thereby relieving the incertitude in choosing binning−thresholding parameters. We characterize this procedure by detecting the two-photon emission bursts from diffusing single gold nanoparticles. The results support our burst-finding procedure as a reliable and efficient way of detecting and harvesting photon bursts from diffusing experiments.

1. Introduction

The ability to observe individual fluorescent molecules or particles as they move across a sensing region opens up many new possibilities in both basic and applied sciences.[1] More recently, for example, it has allowed probing of protein conformational distribution,[2,3] rapid classification of individual molecules,[4,5] and studies of protein folding,[6,7] to name a few. In these diffusion-type experiments, the state of individual molecules is extracted from the short bursts of photons that are collected, while the randomly moving probe molecule remains in the detection zone in a confocal setup.[8] Despite the fast-paced advances in single-molecule observation,[9−11] to obtain reliable information from the limited number of photons contained in a signal burst remains challenging.[12]

To illustrate the problem at hand, one considers the traces shown in Figure 1, which simulates a typical diffusion experiment. The number of detected photon is displayed as a function of time as a single chromophore traversing through a confocal detection zone (simulation details are in the Appendix). Visual inspection of the traces quickly establishes that, qualitatively, the ∼0.6 s peak is likely a valid signal burst. There are, however, two lesser-intense peaks at ∼0.22 and ∼0.48 s that may also be considered as signal, depending on the extent of smoothing (binning). A hard threshold is typically used to discriminate signal against background noise. To minimize potential false-positive detection, its magnitude can be determined by asserting that no bursts are picked up from a control,[13−16] or the threshold may be adjusted such that the harvested burst size distribution matches with that of a theoretical model.[17] Further filtering and heuristically imposing a minimal burst size are often needed when dealing with such Poisson-distributed photon-counting data. Unlike ensemble-averaged experiments, optical single-molecule studies rely on few photons to determine a physical observable. Therefore, the more photons are available, the more accurately a measurement can be made. Subjective choice of bin width and/or smoothing parameters may impact on the ability to extract useful information from the noisy data.

Generally, one is concerned with the following issues in the detection of diffusing chromophores. (1) Quantitative: The probabilities in erroneously assigning a false-positive detection are specified. This is critical, for example, in assessing the significance of observed rare events such as reactive intermediates. (2) Robust: Useful information is collected from the data sequence directly with the same statistical significance with as few adjustable parameters as possible. In this way, the collected photon bursts can be placed on a commensurate statistical footing. (3) Efficient: Knowledge is extracted from the data sequence by gathering as many information-rich photons as possible.

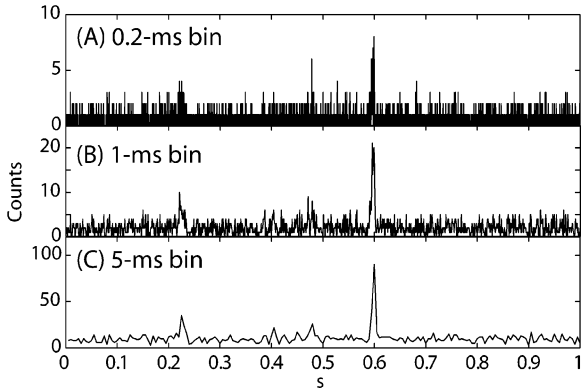

Figure 1. A simulated photon burst as a single molecule/particle traverses through the optical detection zone. Detected photon trace binned at (A) 0.2 ms, (B) 1 ms, and (C) 5 ms. The Poissonian counting noise is evident.

In this article, we present a general procedure that affords reliable detection and efficient collection of emission bursts from single chromophores. It is based on well-characterized ideas from the statistics literature and addresses the issues posed above. This procedure requires only knowledge of the chromophore brightness and the background level, both can be determined by separated control experiments. The indeterminateness in the assignment of the bin time and of thresholding level is removed because our burst-finding method operates on the data set photon by photon. To demonstrate the application of this procedure and to characterize its performance, it is used to detect multiphoton emission from single diffusing gold

10.1021/jp0546047 CCC: $30.25
Published on Web 10/26/2005

nanoparticles. We found that this new procedure does deliver a superior performance over the commonly used binning−thresholding method. The current work extends to the diffusion-type experiments, our recent efforts in developing photon-by-photon single-molecule methods.[18−20] Here we focus on the first step of extracting information from diffusion-type experimental data—the detection and collection of photon bursts. For post-collection statistical data analysis, interested readers may refer to the many excellent discussions in the literature.[17,21−23]

2. Theoretical Considerations

Without loss of generality, the noisy data sequence to be analyzed is considered to be acquired consecutively in time. The signal strength is represented by $I(t)$, which could be current in electronic signal or photon flux in optical detection. The problem of signal burst detection is mapped onto a sequential hypothesis test problem in statistics.[24,25] One considers the sequential test of a null hypothesis H_B—when there is no signal and the data sequence is at its basal value, $I(t) = I_B$—against a composite alternative H_S—when there is signal and $I(t) = I_S(t) + I_B > I_B$.[26,27] A composite hypothesis test differs from a simple hypothesis test in that the value of $I_S(t)$ is not specified for the former, but is defined by a range of acceptable values. Following Wald,[27] a composite hypothesis test can be re-formulated as a simple hypothesis test of H_B: $I(t) = I_B$ against H_1: $I(t) = I_1$, where $I_1 > I_B$ is the minimum intensity that is considered "signal" in practice. In the following development, both I_0 and I_B are considered known from separate control experiments or, more conveniently, from the data sequence directly.

Since the recorded data sequence is corrupted by measurement noise, it will take many data elements to determine $I(t)$ to a certain statistical accuracy. This means that a decision about $I(t)$ cannot be made "instantaneously" but requires some finite time interval, $\bar{t}$, during which one has no knowledge if an analyte is in the detection zone. This leads to a coarse-grained (in time) picture that, before a decision can be made within $\bar{t}$, the data elements are assumed to be collected from the same state and are, therefore, identically independently distributed.

Within this framework, the errors in signal burst detection are false detection (type-I error), the probability of which is defined by $\alpha = P(H_1|H_B)$, and missing signal bursts (type-II error), the probability of which is defined by $\beta = P(H_B|H_1)$. One seeks a general approach that conservatively detects signal burst with $\alpha \rightarrow 0$, or, in practice, setting $\alpha = 1/N$, where N is the number of data points. It should also be proficient in signal detection such that the information-rich regions can be correctly identified and isolated. Furthermore, the sought procedure should be robust and does not require additional parameter adjustments or optimizations for different experiments.

2.1. Formulation of a General Algorithm for Determination of Signal Bursts. Here, a simple and effective procedure is proposed to quantitatively detect signal bursts and to efficiently harvest them from a recorded data sequence, $\{\Delta_i\}$. It is based on the sequential probability ratio test (SPRT) by Wald[27] and on the cumulative sum (CUSUM) scheme by Page.[28] These well studied statistical methods are briefly explained below. Wald's SPRT allows one to test hypotheses with given type-I (α) and type-II (β) error rates:[27]

$$\left.\begin{array}{ll} \Lambda_n \le B, & \text{accept } H_B \\ \Lambda_n \ge A, & \text{accept } H_1 \\ B \le \Lambda_n \le A, & \text{take an additional data point,} \end{array}\right\} \quad (1)$$

where $B = \beta/(1-\alpha)$ and $A = (1-\beta)/\alpha$. Λ_n is the likelihood ratio of n data points, defined as $\Lambda_n \equiv \prod_{i=1}^{n} f_1(\Delta_i)/\prod_{i=1}^{n} f_B(\Delta_i)$, where $f_\theta(\Delta_i) \equiv f(\Delta_i|I_\theta)$ is the probability density of acquiring the i-th data point Δ_i, conditioning on I_θ with $\theta = B$ ($\theta = 1$) denoting the background (signal) state. The null hypothesis H_B is accepted when the likelihood ratio Λ_n is less than the critical value B; conversely, the alternative hypothesis H_1 is accepted when the likelihood ratio is greater than A. When there is insufficient evidence contained in the n data points to make a decision, an additional data point is included in the decision making process. In the current application, the SPRT is restarted from the boundary A (or B) once a decision is reached for H_1 (or H_B).

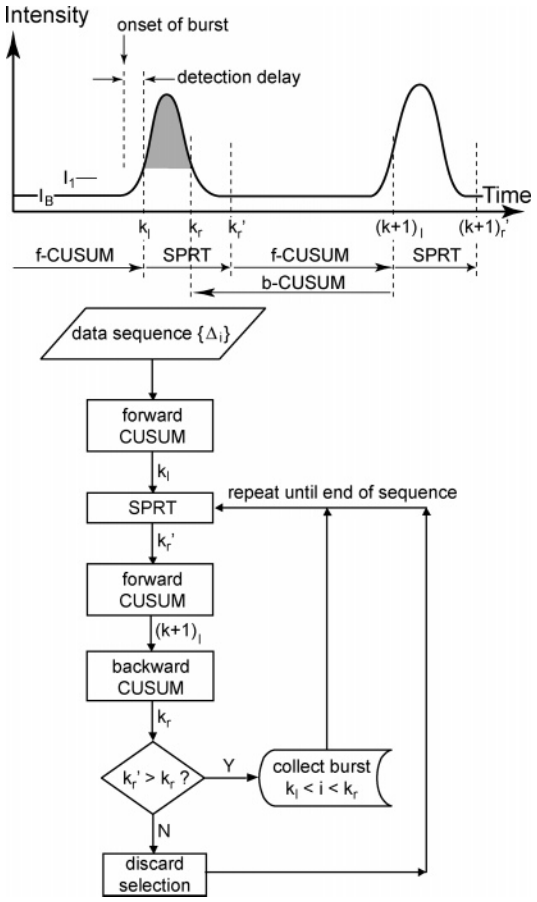

Figure 2. An illustration depicting the proposed forward−backward CUSUM signal burst detection/collection scheme.

Page's CUSUM scheme in its recursive form is

$$\left.\begin{array}{ll} S_0 = 0 & \text{initialization} \\ S_n = \max\left\{S_{n-1} + \ln\left[\dfrac{f_1(\Delta_n)}{f_B(\Delta_n)}\right], 0\right\} & \text{for } n \ge 1 \\ S_n \ge h, & \text{burst detected} \end{array}\right\} \quad (2)$$

where h defines the critical region of burst detection. Page has pointed out that the CUSUM algorithm is essentially a repeated Wald's SPRT with boundaries at 0 and h instead of A and B.[28] This can be seen in the second statement of eq 2, where a new SPRT is started whenever S_n is reset to 0.

The procedure proposed here combines these two rigorous statistical methods to allow efficient detection and conservative collection of signal bursts. The algorithm is summarized in Figure 2. The onset of the k-th burst, k_l, is detected by a CUSUM scheme that analyzes data sequentially (forward CUSUM, or f-CUSUM). The approximate trailing edge of this signal burst, k_r', is located by application of Wald's SPRT. Note that, at this

point, the signal burst defined by $\{\Delta_{k_l},...,\Delta_{k_r'}\}$ is not a conservative collection because k_r' most likely overestimates the trailing edge. Indeed, the expected delay in detecting $I_1 \rightarrow I_B$ using SPRT is greater than 0 and is bound both by the error rates as well as by the expectation value of the log-likelihood ratio, $\lambda(\Delta) \equiv \ln[f_1(\Delta)/f_B(\Delta)]$,[27]

$$E_{I_1 \rightarrow I_B}(n_d) \geq \frac{1}{\langle\lambda\rangle_B}[(1-\alpha)\ln B + \alpha \ln A] \tag{3}$$

where the detection delay n_d is expressed in terms of number of data points and $\langle\lambda\rangle_B = \int_0^\infty \lambda(\Delta) f_B(\Delta) d\Delta$. As will become clear later, the expectation value of the log-likelihood ratio plays a crucial role in the performance of sequential analysis.

To find a conservative set of signal burst, we proceed to find the onset of the next $(k+1)$-th burst using *f*-CUSUM. This is followed by a reverse-chronological CUSUM (backward CUSUM, or *b*-CUSUM) to locate k_r to ensure that the harvested signal burst is conservative and does not contain data points from the background region. In *b*-CUSUM, statistical tests are applied in the reverse sequence order: $\{\Delta_{(k+1)_l}, \Delta_{(k+1)_l-1},...\}$. Signal burst collection is considered successful if $k_l < k_r$.

The CUSUM scheme has many advantageous properties which include, by eq 2, its ease of implementation and efficiency in computing resources. More importantly, the worse-case detection delay (cf. Figure 2) is minimized given the constraint of fixed false-alarm rate α.[29−32] Here, one is interested in such a conservative burst detection that no false-alarm is signaled for the entire trace of N photons; that is, $\alpha \leq N^{-1}$. Under this condition, the optimal value for the threshold h in eq 2 exists and is give by Lorden[31]

$$\exp[-h] = \frac{\alpha \ln[\alpha^{-1}]}{3[\langle\lambda\rangle_1 + 1]^2} \tag{4}$$

where $\langle\lambda\rangle_1 = \int_0^\infty \lambda(\Delta) f_1(\Delta) d\Delta$ is the expectation value of λ when data are drawn from the signal probability density function. The corresponding expected detection delay is[31]

$$E_{I_B \rightarrow I_1}(n_d) \geq \frac{\ln[\alpha^{-1}]}{\langle\lambda\rangle_1}. \tag{5}$$

A shorter detection delay is expected with a greater type-I error rate (greater α, more false-positive detection) and/or a greater $\langle\lambda\rangle_1$. In fact, $\langle\lambda\rangle_1$ can be identified with the Kullback−Leibler discrimination information (or relative entropy, Kullback−Leibler distance), $\mathscr{D}(I_1||I_B)$,[33] which evaluates the extent to which two distributions differ. The greater the difference between I_1 and I_B, the larger the $\langle\lambda\rangle_1$. Therefore, from the information theoretical perspective, $\mathscr{D}$ provides a quantitative understanding of how the signal-to-background ratio affects the quality of the burst detection and collection (cf. eqs 4 and 5).

The procedure outlined above is generally applicable to the identification and collection of signal bursts from a noisy data sequence. The algorithm is formulated such that the framework can be easily implemented for real-time control and on-line analysis. Application of this procedure only requires knowledge of f_B and f_S, the probability densities of background noise and signal, respectively. Both can be obtained accurately by separated control experiments. As an illustration, the next section describes its application to the detection of single fluorescent molecule diffusing through a confocal detection zone.

2.2. Application: Harvesting Emission Bursts from Diffusing Single Chromophores Photon by Photon. One considers an experimental arrangement where a solution containing dilute (few picomolar) fluorescently labeled analyte is to be examined. The solution is interrogated by a laser beam focused via a high numerical aperture (N.A.) microscope objective to form a diffraction-limited excitation volume. The same objective is used to collect the fluorescence photons from the excitation/detection volume (hereafter referred as the detection zone, ζ, see Figure 3A for an illustration). Assuming that the laser excitation direction is along the z axis, ζ is approximated by[34]

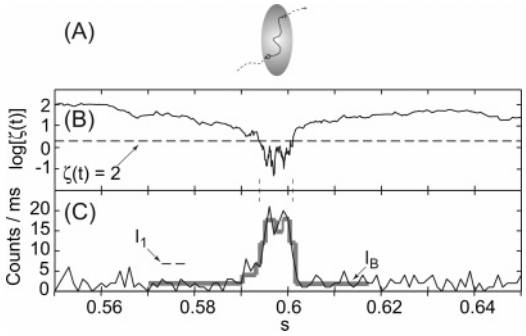

Figure 3. (A) An illustration depicting the detection zone $\zeta(\mathbf{r}_t) \leq 2$ (shaded area), and a diffusing single molecule traversing through it. (B) A simulated position trajectory showing how $\zeta([\mathbf{r}_t)$ varies as the test particle entering and leaving the detection zone. The test particle is considered to be inside the detection zone when $\zeta(\mathbf{r}_t) \leq 2$, indicated by the horizontal dashed line. (C) A simulated photon burst as a single molecule/particle traverses through the optical detection zone. With $I_0 = 20\,000$ and $I_B = 2000$, I_1 is found to be ≈4707 using eq 7.

$$\zeta(\mathbf{r}) = \frac{r_x^2}{\frac{1}{2}w_0^2} + \frac{r_y^2}{\frac{1}{2}w_0^2} + \frac{r_z^2}{\frac{1}{2}z_0^2} \leq 2$$

for one-photon applications. The center of the ellipsoid is assumed (0, 0, 0), and w_0 and z_0 are the minor and major axes of the detection prolate ellipsoid, respectively. The detection zone for two-photon applications can be approximated by a Gaussian−Lorentzian form[35]

$$\zeta(\mathbf{r}) = \frac{2(r_x^2 + r_y^2)}{w^2(r_z)} - \ln\frac{2w_0^2}{\pi w^2(r_z)} \leq 2 \tag{6}$$

where $w^2(r_z) = w_0^2(1 + (r_z/z_R)^2)$, with $z_R = \pi w_0^2/\lambda_{ex}$ and λ_{ex} the excitation wavelength. The apparent instantaneous photon flux due to the test particle at $\mathbf{r}_t(r_x, r_y, r_z)$ is $I_S(t) = I_0 \exp[-\zeta(\mathbf{r}_t)]$, where I_0 is the detected photon flux when the emitting molecule rests at the origin, the center of focus. The total detected photon flux is thus $I(t) = I_S(t) + I_B$, where background photon flux I_B may result from dark counts of the detector or Raman scattering from the medium and is considered constant. In practice, I_B can be measured from control experiments and I_0 can be measured from an immobilized molecule.

A burst of photons is detected when a single fluorescent analyte passes through the detection zone. The waiting times between consecutive photon detection events, Δ, are recorded and stored for analysis. The probability density for detecting Δ given a detectable intensity I is given by $f(\Delta) = I \exp[-\Delta I]$. In other words, the detected inter-photon duration sequence, $\{\Delta\}$, is the stochastic realization of the time-dependent intensity trajectory of a single molecule as it traverses through the detection zone (cf. Figure 1).

As discussed earlier, the efficiency of photon burst detection is largely governed by the threshold intensity, I_1. It can be determined based on the type of sample to be analyzed. If all

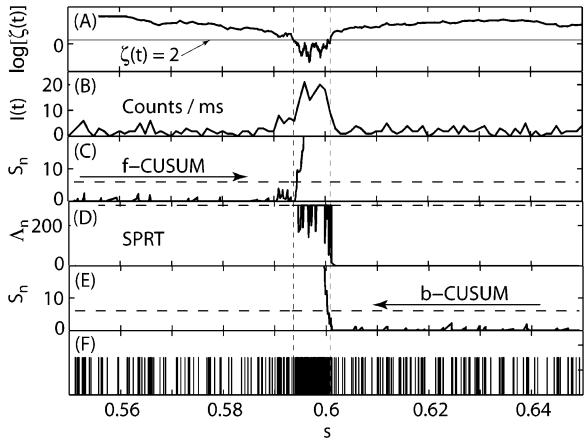

Figure 4. Illustration for the application of the proposed forward−backward CUSUM photon burst detection and collection scheme at various stages. Dashed vertical lines indicate the time instances at which the molecule enters the detection zone defined by $\zeta(t) \leq 2$. (A) A time trajectory of the distance from the focal center of a diffusing molecule traversing through the detection zone. (B) A 1 ms binned emission time trace. (C) The cumulative sum, S_n, in the *f*-CUSUM step as a function of time (cf. eq 2). (D) The likelihood ratio, Λ_n, in the SPRT step as a function of time (cf. eq 1). (E) The cumulative sum, S_n, in the *b*-CUSUM step as a function of time (cf. eq 2). In this step, the CUSUM scheme is applied in a reverse chronological order. (F) The raw, noisy data stream, where each vertical bar represents the arrival of a detected photon. The information-rich photon burst region is visually identified by the densely marked region around 0.59−0.6 s.

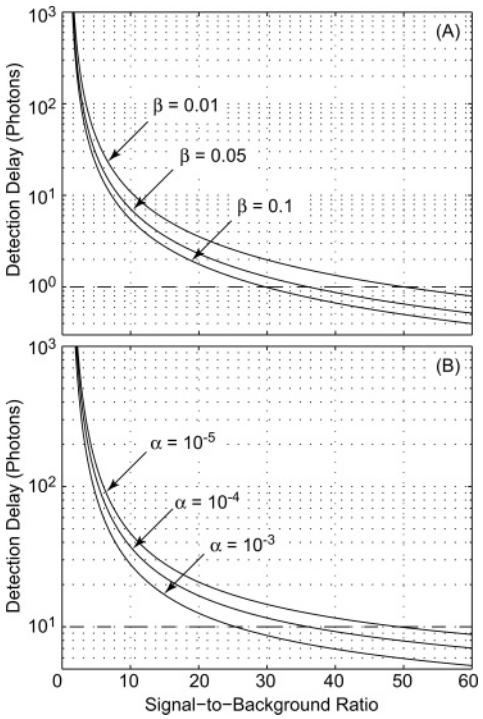

Figure 5. Number of photons necessary to detect a single-molecule burst as a function of signal-to-background ratio under various significance levels. Delay in the detection of a photon burst (A) trailing edge (eq 3 with $\alpha = 10^{-4}$) and (B) onset (eq 5). The α values in (B) correspond to single-molecule time traces of 10^3, 10^4, and 10^5 photons ($\alpha \equiv 1/N$).

the fluorescent species under investigation exhibit comparable I_0, one may consider I_1 to be the most-likely photon flux when the analyte is inside the confocal detection zone, defined by

$$I_1 \equiv I_0 e^{-2} + I_B \tag{7}$$

Alternatively, if the sample contains many species of drastically dissimilar emission properties, one may determine I_1 using eq 5. In this way, statistically, each harvested photon cluster has the same delay in burst detection. With a given detection delay, I_1 is set by the error rate α and the background intensity I_B. The same procedure can be reliably applied to samples of different characteristics.

Application of the proposed procedure is illustrated using the simulated data in Figure 3 and is summarized in Figure 4. Note that the idea of coarse-graining in time is illustrated by the stepwise thick gray lines in Figure 3C, which represent measurable intensity states. Panels B and C from Figure 3 are reproduced here for comparison. This data set contains a total of $N = 316$ photons; therefore, $\alpha = N^{-1} = 3.16 \times 10^{-3}$. From the binned trace (Figure 4), the background and signal intensities are estimated to be $I_B \sim 3200$ cps and $I_0 \sim 23\,000$ cps, respectively. Using eq 7, the threshold intensity is found to be $I_1 \sim 6313$ cps. The Kullback−Leibler discrimination information is $\mathscr{D}(I_1||I_B) \sim 0.57$, whereas the CUSUM boundary is $h = 6.01$ (eq 4). Figure 4C shows the trace of *f*-CUSUM statistic, S_n, as a function of time. S_n crosses h (dashed horizontal line) at $t = 0.5945$ s, which amounts to a detection delay of only 8 photons from the "true" burst onset (vertical dashed line at $t = 0.5940$ s). Switching to SPRT for the approximate trailing edge of the burst (Figure 4D), a type-II error rate of $\beta = 0.05$ was used to give the SPRT bounds $A = 300.2$ and $B = 5.016 \times 10^{-2}$ (horizontal dashed lines in Figure 4D). The burst was found to end at $t = 0.602$ s, exceeding the true end point (vertical dashed line at $t = 0.6010$ s) by 5 photons. To find a conservative set of signal photons, *b*-CUSUM is performed (Figure 4), which crossed the threshold at $t = 0.6002$ s, 9 photons left to the true end point. Our proposed procedure thus conservatively harvests 99 photons for this particular data set.

More generally, the efficiency of photon burst detection can be characterized using the analytical expressions for expected delay in burst detection (eqs 3 and 5). Representative results are displayed in Figure 5. As expected, when the signal-to-background ratio (S/B) is low, a great number of photons are needed to successfully identify the presence of a burst with sufficient statistical significance. The more stringent the error rates are, the greater the S/B is required to detect the trailing edge (or the onset) of a photon burst. For example, as illustrated in Figure 5A, Wald's SPRT is able to identify the trailing edge with only 1 photon if the S/B is greater than 30. On the other hand, since we are interested in a conservative photon burst collection such that the false-positive is ∼0, it will take more photons to detect the onset of a photon burst. For an S/B ∼ 30 and a trajectory of 10 000 photons, it will take more than 10 photons to correctly identify the onset of a burst.

Figure 5 also sheds light on the effectiveness of resolving two consecutive bursts. Under typical experimental conditions, more than 10 photons will be required to resolve two adjacent bursts. Despite the fact that the present general method operates on a photon-by-photon basis, it is still unlikely to resolve multiple photon bursts that result from an analyte molecule rapidly coming in and out of the detection zone. This aspect is important when treating chemically reactive systems. For example, detection of bursts resulting from product released by a single reactive molecule is likely to be biased toward infrequent product formation events. This also highlights the challenges in recovering the full distribution of burst duration and inter-burst waiting times in a statistically reliable manner. Further development in post-burst-collection analysis, which is

underway in our laboratory, is expected to help address issues of this nature.

3. Experiment

As a demonstration, this new procedure is used to acquire multiphoton emission signal from gold nanoparticles as they diffuse through the focal volume. The photostability and the expected fast radiative decay rate of gold nanostructures[36−38] allow a convenient assessment for the effectiveness of our method. Furthermore, recent studies have suggested the use of colloidal metal particles as a contrasting agent in imaging.[39−43] These, together with advances in nanoparticle−protein one-to-one conjugation,[44] lead us to suppose that metallic colloids may be used for rapid and quantitative analysis that could find applications in toxicant detection and in diagnosis. The feasibility of using our new method to count particles as a way to quantify concentration is also tested.

3.1. Materials and Procedures. The 60 nm gold nanoparticle solution was purchased from Ted Pella and used as received (stock solution). The blank for control experiments was prepared using the same solution but without gold particles. To remove the particles, an aliquot of 10X dilution from the stock was concentrated at a relative centrifugal force (RCF) of 20 800 for 15 min (Eppendorf 5417C). The supernatant was immediately collected for subsequent experiments. To prepare samples of immobilized gold nanoparticles, 1 mL stock solution was concentrated by 15 min centrifugation at 720 RCF. About 950 μL of the supernatant was discarded, and the remaining ~50 μL of concentrated solution was resuspended in filtered water (Barnstead NANOPure DIamond UV/UF, pH ~ 5.5−6) to 1 mL. Ten microliters of the above solution was spin-coated on cleaned quartz coverslips (Technical Glass) at 3500 rpm for 10 s (Laurell, WS-400B-6NPP/LITE/8K). This procedure produced a typical coating density of about 2−4 particles per 10 × 10 μm^2. The sample was enclosed by an imaging chamber (CoverWell, Invitrogen) following addition of 20 μL filtered water. In burst detection experiment, an aliquot of received stock solution was diluted using filtered water to the desired concentration. A UV−vis spectrometer (HP 8453) was used to calibrate the sample concentrations, using a vendor-supplied extinction coefficient of ϵ(520 nm) = 2.79 × 10^{10} cm^{-1} M^{-1}. The picomolar sample was also contained in a chamber made of a quartz coverslip and a CoverWell seal.

The details of the experimental setup have been described elsewhere.[45] Briefly, the ~70 fs excitation pulses at 800 nm were generated by a broad-band Ti:sapphire oscillator (Spectral Physics Tsunami), which was pumped by a frequency-doubled diode laser (Spectral Physics Millennia Xs J). The excitation pulses are guided into a microscope (Olympus IX71) and reflected by a short-pass dichroic filter (Chroma 650DCSX) to focus at the sample through a microscope objective (Leica HCX Plan Apo CS, 100X, 1.40−0.7 NA, oil immersion). To set the signal intensity I_0, surface-immobilized samples were first characterized. A piezo stage (Physik Instrumente PI-577.3CL) was used to raster scan for gold particles, from which I_0 was measured. For diffusion-type experiments, the focal plane was adjusted such that it is far away from the quartz coverslip. Multiphoton luminescence was collected by the same objective, sent through two emission filters (Chroma, E480LP and E680SP), and detected by a single-photon counting avalanche photodiode (Perkin-Elmer ACQR-140). Sequences of photon detection events were time-stamped using a time-correlated single-photon counting (TCSPC) card (Becker-Hickl SPC-630) and recorded by a personal computer for later analysis.[46] The instrument response (~450 ps) was measured using the reflected laser light from a quartz−air interface with the emission filters removed. The average laser power at the sample was maintained at 2.3 mW such that the detection process was still within single photon counting regime. A 15 min trajectory was generated for each measurement and repeated at least five times for each concentration.

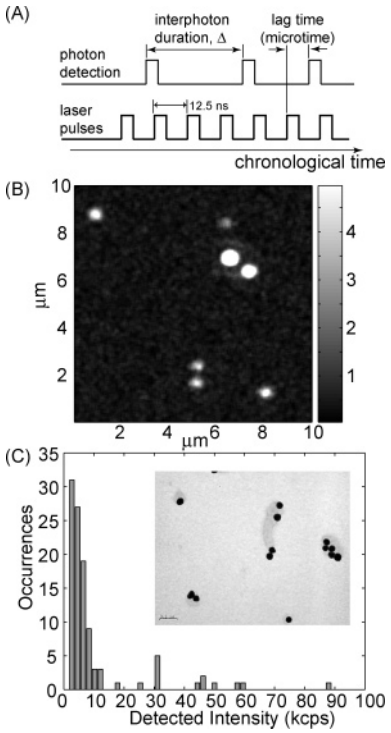

Figure 6. (A) Timing scheme for the time-stamped TCSPC experiments. The inter-photon durations {Δ} are used to estimate emission intensity, and the time lags are used to estimate excited-state lifetime. (B) A raster-scanned image of 60 nm gold nanoparticles on a quartz coverslip. A 5 × 5 pixel^2 Gaussian filter was used for presentation purposes. The linear scale is adjusted such that dim particles are visible. Images like this were used to calibrate the I_0 for use in the burst-finding algorithm. For example, the brightness of the particles shown on this image can be approximately categorized into four levels. They are 1.7, 3.2, 4.9, and 8.2 kcps. (C) Distribution of observed brightness over 106 particles. The most probable intensity peaks at about 3.2 kcps. Inset: A TEM image of 60 nm gold particles showing variations in shape, orientation, and possibly aggregates (scale bar at the bottom-left corner: 200 nm). These factors are likely to contribute to the distribution in the observed multiphoton emission.

3.2. Results and Discussion. Two parameters are required for the extraction of burst signals photon by photon. They are the background level, I_B, and the brightness of the chromophore, I_0. The former can be measured from control experiments of a blank solution and the latter from individual nanoparticles immobilized on a quartz coverslip. A representative image used for I_0 determination is shown in Figure 6A. When parked on individual particles for extended data acquisition, no photodegradation was observed during the ~2 min imaging period. The power dependence of photoluminescence from this collection of particles ranges from 2.0 to 2.3. The emission spectrum is also consistent with that from 410 nm one-photon excitation, indicating a two-photon process populating the 3.02 eV band reported by Varnavski et al.[37] Statistical analysis of I_0 from 106 particles showed a distribution of intensity levels. This is likely due to variations in particle size and shape, as well as due to possible nonspecific association. The most probable intensity from the distribution was used for photon burst detection, setting I_0 ~ 3.2 kcps.

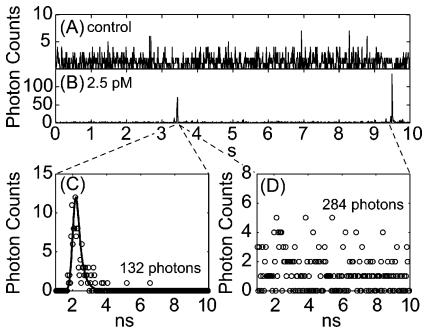

Figure 7. (A) A typical 10 s intensity trace from a blank sample, binned at 10 ms. (B) A 10 ms binned time trace from a 2.5 pM sample showing two photon bursts originating from gold nanoparticles diffusing through the focal volume. For this particular sample, a total of 117 bursts were harvested from a 15 min trajectory. (C) Radiative decay constructed from the indicated photon burst. The solid line is an instrument response. (D) Radiative decay trace constructed from the indicated region where there is no signal burst.

A portion of the time trace from a control experiment of blank sample is shown in Figure 7A. It gives an average photon count of $I_B \sim 120$ cps, basically the dark count rate of the APD. Together with I_0 determined earlier this gives a signal-to-background ratio of ~28. The expected detection delay was found to be about 11 photons (cf. eqs 7 and 5 and Figure 5). No signal bursts were identified when applying our burst-finding algorithm to data acquired from blank samples. A typical time trace for nanoparticle-containing solution is shown in Figure 7B. The two visible signal bursts were readily identified by our method. The excited-state lifetime from these fleeting nanoparticles was measured by constructing a histogram of the time lag between the excitation pulse and the photon arrival time.[47−50] Displayed in Figure 7C is such a histogram constructed using photons harvested from the indicated burst. It shows a detector-limited radiative decay, as indicated by the overlaid instrument response curve. Heterogeneity in the radiative decay is also observed and is tentatively attributed to the nonuniformity of the sample as well as to the uncertainties in the lifetime fitting. This, however, does not affect our use of lag-time histogram to characterize the performance of our new method. The background region of a time trace is also easily identified. Their lag-time histograms appear uniformly distributed, as expected from APD dark count and incoherent scattering light (cf. Figure 7D). Such a sharp contrast in lag-time histogram allows us to assess the effectiveness of our burst-finding method. Since the determination of signal bursts from a data sequence can also be considered as a binary classification between signal and background regions, gold nanoparticle emission photons that are not identified as signal (misclassified) will appear as a pronounced peak in the background lag-time histogram.

To evaluate the effectiveness of our photon-by-photon approach, we compared it with a simple binning−thresholding method. A time trace of length T is binned with δ to give a total of $N_b = T/\delta$ time bins. The probability density of detecting n photons in each time bin from a blank experiment is given by a Poisson distribution, $\mathrm{Poi}(n|I_B) = (I_B)^n \exp[-I_B]/n!$. To define the threshold, n_{th}, that classifies a binned trajectory into regions of signal or background, one considers a false-positive error rate, $\alpha_{\mathrm{th}} = 1/N_b$. The comparison is made for each time bin. In this way, at most, one false-positive identification is made if the sample is blank. This is in the same spirit as the error rate used in the photon-by-photon approach ($\alpha = 1/N$), where, at most, one false-positive photon is assigned; n_{th} can be found numerically by solving the equation, $\sum_{n=0}^{n_{\mathrm{th}}} Poi(n|I_B) = 1 - \alpha_{\mathrm{th}}$. The results are displayed in Figure 8. Pronounced population

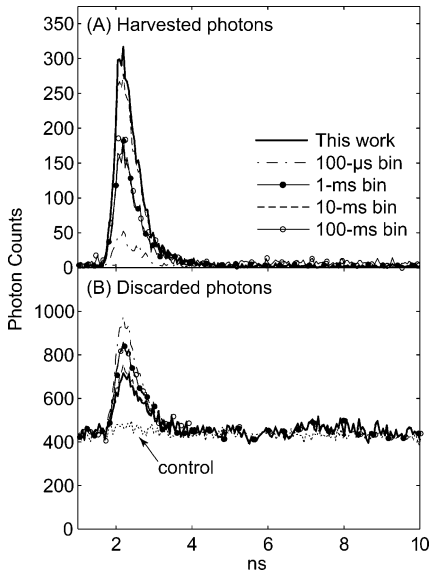

Figure 8. (A) Lag-time histogram of harvested photons from the 2.5 pM sample shown in Figure 7, suggesting that the photon-by-photon method (thick black line) is indeed more efficient compared to the binning−thresholding method at various bin times. (B) Lag-time histogram of photons from the background regions, showing that the photon-by-photon method does not lose too much information from misclassifying signal photons to background and compares admirably with the binning−thresholding method.

at around 2 ns in the lag-time histogram indicates successful collection of information-rich photons (cf. Figure 8A). The small number of misassigned photons by our burst-finding method is expected (Figure 8B) because of the conservativity criterion that is explicitly built in the procedure (cf. Figure 2). Our new approach appears to be most effective in collecting photons from the information-rich regions compared to the binning−thresholding method at various bin widths. More quantitatively, the effectiveness relative to the photon-by-photon approach in harvesting signal photons can be characterized by comparing the number of photons contained within the 1.5−4.9 ns region. They are 15% for the 100 μs bin, 57% for the 1 ms bin, 91% for the 10-ms bin, and 61% for the 100 ms bin. Note that the burst-finding procedure proposed here achieves the highest efficiency without any variational parametrization.

For potential applications, for example, it would be advantageous in sensing if the analyte concentration can be quantified by simply counting the number of detected bursts. Possible scenarios include applications in capillary electrophoresis, in microfluidic or nanofluidic devices, and in open-volume detection with ultralow analyte concentration. To test the feasibility of using the photon-by-photon method in this type of applications, we have carried out initial experimental characterization for the open-volume case. Results from samples of different concentrations are summarized in Figure 9. A clear linear dependence is observed, with a correlation coefficient $r > 0.99$ for concentrations less than 20 pM. Since the number of bursts detected per unit time is a stochastic variable, it is important to repeat the experiment a few times so that the mean converges. Several factors may contribute to deviation from linearity at higher concentrations. Off-focus chromophores are expected to play a role. Other factors include having more than one particles in the detection zone and the limited resolving power to trace the true trajectory of a chromophore transiently coming in and out of the detection zone. More advanced post-collection statistical analyses are needed to address these issues that are important for treating reactive systems and for studying diffusion

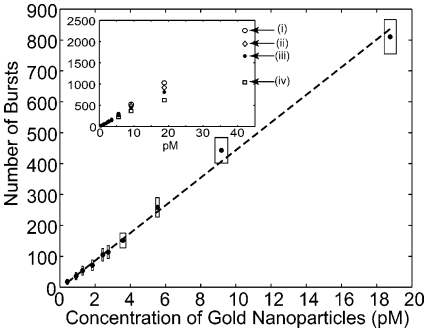

Figure 9. Number of photon bursts detected in 15 min as a function of particle concentration. The error bounds represent 1.96 × standard deviation. (Inset) Number of bursts at four different I_0 values from immobilized measurement (cf. Figure 6). The I_0 values are (i) 8.2 kcps ($r = 0.9995$, $\chi^2 = 0.67$), (ii) 4.9 kcps ($r = 0.9989$, $\chi^2 = 0.69$), (iii) 3.2 kcps ($r = 0.9980$, $\chi^2 = 0.78$), and (iv) 1.7 kcps ($r = 0.9948$, $\chi^2 = 1.35$).

dynamics in disordered media that may exhibit a time-dependent diffusion coefficient.[51,52] Works to extend this approach to multispectral single-molecule spectroscopy is also underway.[53]

Acknowledgment. This work was supported by the Laboratory Directed Research and Development Program of Lawrence Berkeley National Laboratory under U.S. Department of Energy contract No. DE-AC03-76SF00098, and by the University of California at Berkeley. Dr. Carl Hayden of the Sandia National Laboratory is gratefully acknowledged for illuminating discussions. We also thank one of the reviewers for constructive suggestions and for bringing relevant references to our attention.

Appendix: Computer Simulation Details

The computer simulations assumed an idealized situation in which there was, at most, one particle in the detection zone. It was further assumed that the analyte was composed of hard-sphere particles of hydrodynamic diameter, d, that were freely diffusing inside a simulation box of dimension $b \times b \times b$. The periodic boundary condition was imposed during the simulation, in which the size of the simulation box was determined by user-supplied analyte concentration. Under the slip (or nonstick) approximation, the diffusion constant D of a test particle follows the Stokes−Einstein relation at temperature T:

$$D = \frac{k_B T}{2\pi\eta d} \tag{8}$$

where k_B is the Boltzmann constant and η the bulk viscosity of the solvent. On a coarse-grained time scale, δt, the diffusion dynamics can be modeled by the position Langevin equation,[54] in which the propagation of particle position follows[55]

$$\mathbf{r}(t + \delta t) = \mathbf{r}(t) + \delta\mathbf{r}^G, \tag{9}$$

where each component of $\delta\mathbf{r}^G$ is polled from an independently identically distributed Gaussian density with mean 0 and variance $\langle(\delta r_i^G)^2\rangle = 2D\delta t$. Under these conditions, the probability density of detecting one photon at any given instant t is

$$f(t) = I(t)\exp[-I(t)\delta t] \tag{10}$$

In the simulations reported herein, a number a was drawn randomly from a uniform distribution between 0 and 1. A detection event occurred if $a < I(t)\delta t$, when the chronological time t, the inter-photon duration Δ, the particle position $\mathbf{r}$, and the intensities $I_S(t)$ and $I_B(t)$ were recorded. The simulation was terminated when the desired trajectory length has been recorded. For Figure 1, the analyte concentration of this simulation is 10 pM, $d = 10$ nm, $T = 298.15$ K, $\eta = 0.89$ mPa·s (water), $\sigma_x = \sigma_y = 255$ nm, $\sigma_z = 1020$ nm, $I_0 = 20000$ cps, $I_B = 200$ cps, and $\delta t = 1$ μs.

References and Notes

(1) Ambrose, W. P.; Goodwin, P. M.; Jett, J. H.; van Orden, A.; Keller, J. H. W. a. R. A. *Chem. Rev.* **1999**, *99*, 2929.

(2) Rothwell, P. J.; Berger, S.; Kensch, O.; Felekyan, S.; Antonik, M.; Wohrl, B. M.; Restle, T.; Goody, R. S.; Seidel, C. A. M. *Proc. Natl. Acad. Sci. U.S.A.* **2003**, *100*, 1655.

(3) Margittai, M.; Widengren, J.; Schweinberger, E.; Schröder, G. F.; Felekyan, S.; Haustein, E.; König, M.; Fasshauer, D.; Grubmüller, H.; Jahn, R.; Seidel, C. A. M. *Proc. Natl. Acad. Sci. U.S.A.* **2003**, *100*, 15516.

(4) Yeung, E. S. *Annu. Rev. Phys. Chem.* **2004**, *55*, 97.

(5) Kapanidis, A. N.; Lee, N. K.; Laurence, T. A.; Doose, S.; Margeat, E.; Weiss, S. *Proc. Natl. Acad. Sci. U.S.A.* **2004**, *101*, 8936.

(6) Talaga, D. S.; Lau, W. L.; Roder, H.; Tang, J. Y.; Jia, Y. W.; DeGrado, W. F.; Hochstrasser, R. M. *Proc. Natl. Acad. Sci. U.S.A.* **2000**, *97*, 13021.

(7) Schuler, B.; Lipman, E. A.; Eaton, W. A. *Nature* **2002**, *419*, 743.

(8) Haustein, E.; Schwille, P. *Curr. Opin. Struct. Biol.* **2004**, *14*, 531.

(9) Moerner, W.; Fromm, D. *Rev. Sci. Instrum.* **2003**, *74*, 3597.

(10) Xie, X. S.; Trautman, J. K. *Annu. Rev. Phys. Chem.* **1998**, *49*, 441.

(11) Kulzer, F.; Orrit, M. *Annu. Rev. Phys. Chem.* **2004**, *55*, 585.

(12) Lippitz, M.; Kulzer, F.; Orrit, M. *ChemPhysChem* **2005**, *6*, 770.

(13) Peck, K.; Stryer, L.; Glazer, A. N.; Mathies, R. A. *Proc. Natl. Acad. Sci. U.S.A.* **1989**, *86*, 4087.

(14) Enderlein, J.; Robbins, D. L.; Ambrose, W. P.; Goodwin, P. M.; Keller, R. A. *J. Phys. Chem. B* **1997**, *101*, 3626.

(15) Enderlein, J.; Goodwin, P. M.; van Orden, A.; Ambrose, W. P.; Erdmann, R.; Keller, R. A. *Chem. Phys. Lett.* **1997**, *270*, 464.

(16) Eggeling, C.; Berger, S.; Brand, L.; Fries, J.; Schaffer, J.; Volkmer, A.; Seidel, C. *J. Biotechnol.* **2001**, *86*, 163.

(17) Fries, J. R.; Brand, L.; Eggeling, C.; Köllner, M.; Seidel, C. A. M. *J. Phys. Chem. A* **1998**, *102*, 6601.

(18) Watkins, L. P.; Yang, H. *Biophys. J.* **2004**, *86*, 4015.

(19) Watkins, L. P.; Yang, H. *J. Phys. Chem. B* **2005**, *109*, 617.

(20) Watkins, L. P.; Chang, H.; Yang, H. **2005**, submitted.

(21) Ko, D.; Sauer, M.; Nord, S.; Muller, R.; Wolfrum, J. *Chem. Phys. Lett.* **1997**, *269*, 54.

(22) Schröder, G. F.; Grubmüller, H. *J. Chem. Phys.* **2003**, *119*, 9920.

(23) Gopich, I.; Szabo, A. *J. Chem. Phys.* **2005**, *122*, 014707.

(24) Basseville, M.; Nikiforov, I. V. *Detection of Abrupt Changes: Theory and Application*; Prentice Hall: Englewood Cliffs, CA, 1993.

(25) Lai, T. L. *J. R. Stat. Soc. B* **1995**, *57*, 613.

(26) Wald, A. *Ann. Math. Stat.* **1945**, *16*, 117.

(27) Wald, A. *Sequential Analysis*; John Wiley & Sons: New York, 1947.

(28) Page, E. S. *Biometrika* **1954**, *41*, 100.

(29) Lorden, G. *Ann. Math. Stat.* **1971**, *42*, 1897.

(30) Lorden, G. *Ann. Math. Stat.* **1972**, *43*, 1412.

(31) Lorden, G. *Ann. Stat.* **1973**, *1*, 633.

(32) Moustakides, G. V. *Ann. Stat.* **1986**, *14*, 1379.

(33) Kullback, S.; Leibler, R. A. *Ann. Math. Stat.* **1951**, *22*, 79.

(34) Aragon, S. R.; Pecora, R. *J. Chem. Phys.* **1976**, *64*, 1791.

(35) Berland, K. M.; So, P. T. C.; Gratton, E. *Biophys. J.* **1995**, *68*, 694.

(36) Beversluis, M. R.; Bouhelier, A.; Novotny, L. *Phys. Rev. B* **2003**, *68*, 115433.

(37) Varnavski, O. P.; Mohamed, M. B.; El-Sayed, M. A.; Goodson, T. *J. Phys. Chem. B* **2003**, *107*, 3101.

(38) Schuck, P. J.; Fromm, D. P.; Sundaramurthy, A.; Kino, G. S.; Moerner, W. E. *Phys. Rev. Lett.* **2005**, *94*, 017402.

(39) Zheng, J.; Dickson, R. M. *J. Am. Chem. Soc.* **2002**, *124*, 13982.

(40) Zheng, J.; Petty, J. T.; Dickson, R. M. *J. Am. Chem. Soc.* **2003**, *125*, 7780.

(41) Zheng, J.; Zhang, C. W.; Dickson, R. M. *Phys. Rev. Lett.* **2004**, *93*, 077402.

(42) Farrer, R. A.; Butterfield, F. L.; Chen, V. W.; Fourkas, J. T. *Nano Lett.* **2005**, *5*, 1139.

(43) Lippitz, M.; van Dijk, M. A.; Orrit, M. *Nano Lett.* **2005**, *5*, 799.

(44) Aubin, M. E.; Morales, D. G.; Hamad-Schifferli, K. *Nano Lett.* **2005**, *5*, 519.

(45) Zhang, K.; Chang, H.; Fu, A.; Alivisatos, A. P.; Yang, H. **2005**, submitted.
(46) Becker, W.; Hickl, H.; Zander, C.; Drexhage, K. H.; Sauer, M.; Siebert, S.; Wolfrum, J. *Rev. Sci. Instrum.* **1999**, *70*, 1835.
(47) Köllner, M.; Wolfrum, J. *Chem. Phys. Lett.* **1992**, *200*, 199.
(48) Ambrose, W. P.; Goodwin, P. M.; Martin, J. C.; Keller, R. A. *Science* **1994**, *265*, 364.
(49) Xie, X. S.; Dunn, R. C. *Science* **1994**, *265*, 361.
(50) Brand, L.; Eggeling, C.; Zander, C.; Drexhage, K. H.; Seidel, C. A. M. *J. Phys. Chem. A* **1997**, *101*, 4313.
(51) Zwanzig, R. *Chem. Phys. Lett.* **1989**, *164*, 639.
(52) Cao, J. *Phys. Rev. E* **2001**, *63*, 041101.
(53) Luong, A. K.; Gradinaru, C. C.; Chandler, D. W.; Hayden, C. C. *J. Phys. Chem. B* **2005**, *109*, 15691.
(54) Lax, M. *Rev. Mod. Phys.* **1966**, *38*, 541.
(55) Ermak, D. L.; Yeh, Y. *Chem. Phys. Lett.* **1974**, *24*, 243.